Anastasopoulos, I. *et al.* (2013). *Géotechnique* **63**, No. 12, 1042–1059 [http://dx.doi.org/10.1680/geot.12.P.114]

Interaction of piled foundation with a rupturing normal fault

I. ANASTASOPOULOS*, R. KOURKOULIS*, G. GAZETAS* and A. TSATSIS*

Post-seismic observations in the 1999 Kocaeli earthquake in Turkey have indicated that piled foundations may be less suitable than stiff mat foundations in defending a structure against a major normal fault rupturing underneath. This paper explores the interplay of such a rupture, as it propagates in a moderately dense sand stratum, with an embedded two by four pile foundation (typical of common highway overpass bridges). An experimentally validated numerical scheme and constitutive law for sand are utilised in the analysis, with due attention to realistically modelling the non-linear pile–soil interface and the structural inelasticity of the piles. Parametric results identify and elucidate the development of different rupture mechanisms as a function of the exact location of the group relative to the fault and of the magnitude of the tectonic displacement (the fault offset). It is shown that even for a moderate fault offset (less than 0·5 m), lightly reinforced piles will fail structurally, while also forcing the pile cap and the bridge pier on top to undergo substantial rotation and displacement. Even heavy reinforcement might not prevent potentially disastrous displacements. Pile inelasticity is unavoidable and should be acceptable as part of a ductility-based design. However, despite the possible survival of the piles themselves, letting them reach the limit of their ductility capacity may lead to large cap rotation and displacements, which are likely to impose severe demands on the superstructure. Piled foundations may indeed be inferior to rigid raft foundations in protecting a structure straddling an active seismic fault, but with few notable exceptions.

KEYWORDS: earthquakes; piles; numerical modelling; soil/structure interaction

INTRODUCTION

In the destructive Kocaeli M_W 7·5 earthquake of August 1999, the village of Denizevler (near the devastated city of Gölcük) was crossed by a normal fault rupture, the vertical offset of which reached up to 2·5 m on the ground surface. Several three- to five-storey buildings survived nearly unscathed the offset, as their rigid raft foundations 'forced' the fault rupture to divert around their periphery, leaving them either on top (footwall) or in the bottom (hanging wall) of the normal scarp. This was an astonishing success for non-professionally engineered structures, although admittedly (a) the fault, if it were unperturbed, would only have ruptured underneath a small part of them, near a corner and (b) the soft nature of the underlying silty soil had also (fortuitously) contributed to their success (Anastasopoulos & Gazetas, 2007).

A few hundred metres away, the newly built Atatturk basketball stadium was not so fortunate, although it had also been crossed by the fault just at one of its corners and, moreover, the rupture offset was smaller, about 1·5 m (only). As shown in Fig. 1, not only did the outside piles crack (flexurally) near their head, but their outward and downward movement triggered major diagonal cracks on the supported superstructure. No other damage due to seismic shaking was visible; yet, the stadium was condemned to demolition.

This and some additional scant (and admittedly rather circumstantial) evidence from the three notorious 1999 earthquakes of Kocaeli, Düzce and Chi-Chi has implicated the piles in observed structural damage (Youd *et al.*, 2000; Kawashima, 2001; Ulusay *et al.*, 2002 ; Bray, 2005; Anastasopoulos & Gazetas, 2007; Faccioli *et al.*, 2008). It appears that foundation systems 'tied' to the two blocks of a fault (the so-called hanging wall and footwall) may indeed be vulnerable. This may be the case with a group of piles. An interesting analogy has been suggested in a lecture by Professor Jonathan Bray (2005): deep-rooted trees were torn apart, splitting in two, by a strike–slip fault rupturing underneath, apparently as a result of their roots having been pulled apart by the two opposite blocks of the fault.

In view of the important use of piles to protect structures against total and differential settlements, their role in supporting structures straddling seismic faults deserves a theoretical investigation, such as the one presented in this paper. A similar study on embedded caisson foundations interacting with a rupturing normal fault has been recently presented in this journal by Loli *et al.* (2012). To the present authors' knowledge, however, no such study has been published to date for piled foundations.

PROBLEM DEFINITION AND METHODOLOGY

Figure 2 represents schematically the main features of the problem geometry and defines the coordinate system. The foundation consists of a group of 2×4 reinforced-concrete bored piles with diameter $d = 1{\cdot}2$ m and length $D = 18$ m. Pile spacing is equal to three diameters (i.e. 3·6 m), and the parametrically variable amount of reinforcement ranges from $\rho = 1\%$ to 4% ratio of steel over concrete cross-sectional area. The cap is a rigid slab having dimensions $L = 13$ m and $B = 6$ m in the longitudinal and transverse directions, respectively. The depth of the soil stratum is $H = 22$ m, leaving 4 m of soil between pile tips and base rock – a choice reflecting (admittedly) the computational limitations of the three-dimensional (3D) analysis, but also a technical desire to avoid embedding the piles at bedrock in two different blocks of the fault.

A normal fault at an angle $\alpha = 60°$ to the horizontal undergoes an offset (tectonic dislocation) Δ at the base rock. Caused by a major seismic event, Δ is varied parametrically

Manuscript received 4 August 2012; revised manuscript accepted 28 February 2013. Published online ahead of print 19 April 2013. Discussion on this paper closes on 1 February 2014, for further details see p. ii.

*Laboratory of Soil Mechanics, National Technical University, Athens, Greece.

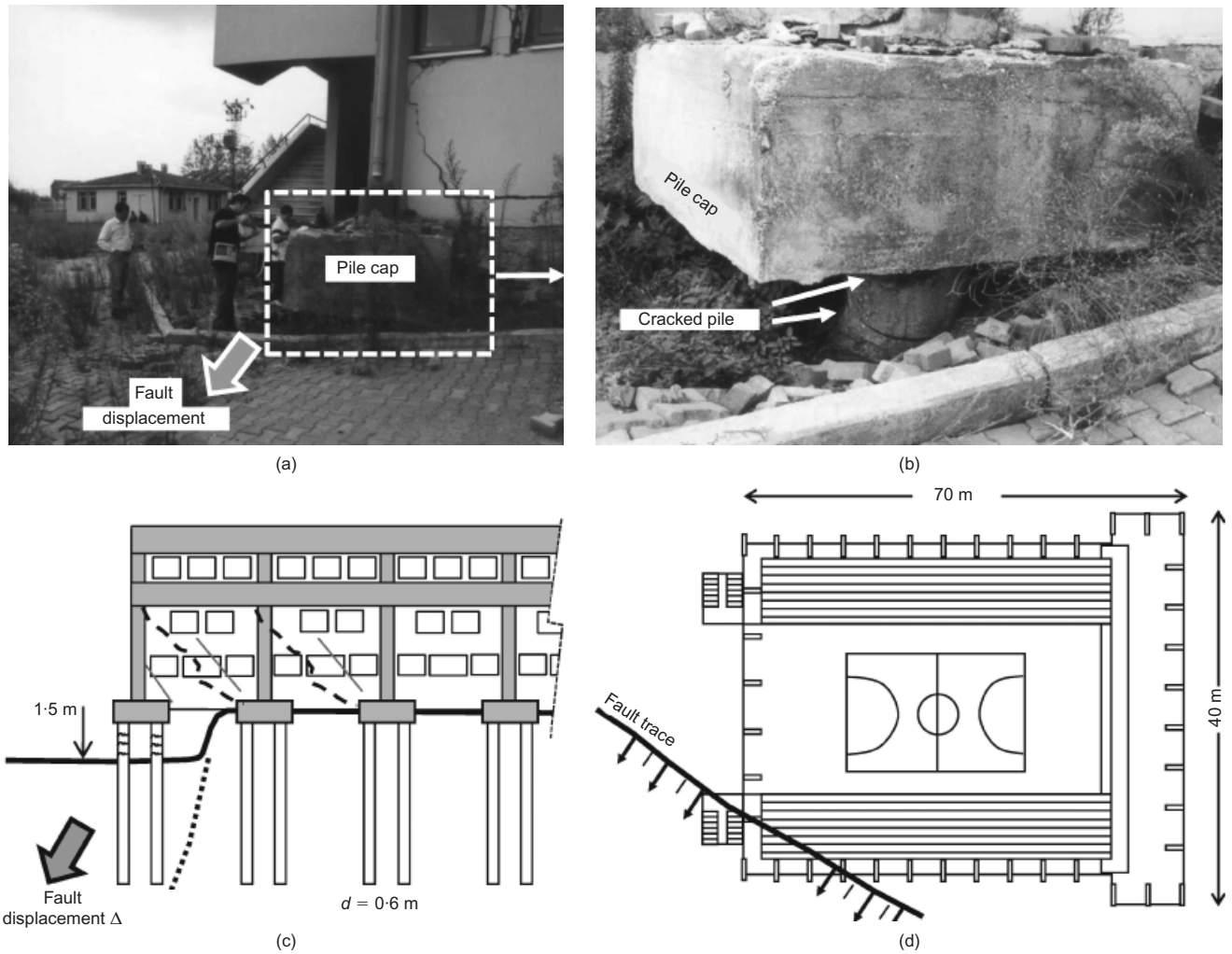

Fig. 1. Basketball stadium in Denizevler: (a) photograph of the building's corner crossed by the fault trace; (b) zoomed view showing the failed piles; (c) schematic cross-section; (d) plan view of the building along with the fault trace

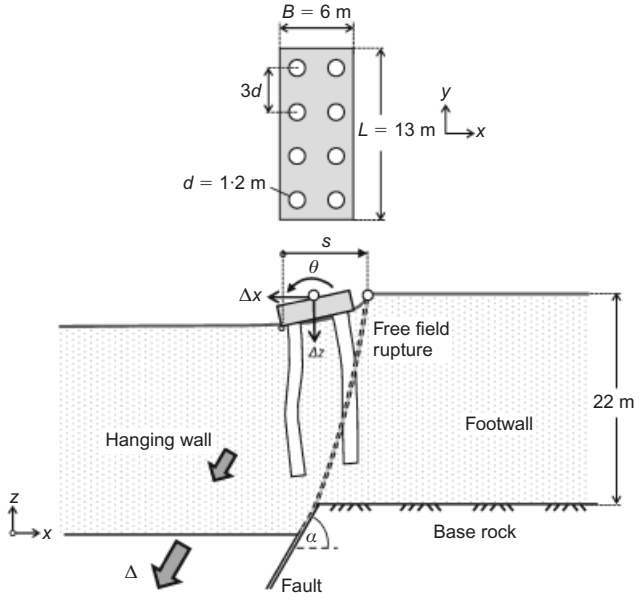

Fig. 2. Schematic illustration of the studied 2 × 4 pile group

in this study. The vertical component $h = \Delta \sin\alpha$ is used as a measure of the dislocation size; it is varied between a small $h = 0{\cdot}2$ m to a substantial $h = 1{\cdot}0$ m.

When no structure or foundation is present, the fault rupture propagates upward from the base, with the deformation localising along a single rupture surface and, eventually, if h is sufficiently large, emerging on the surface (Cole & Lade, 1984; Lade *et al.*, 1984; Bray *et al.*, 1994a, 1994b; Anastasopoulos *et al.*, 2007). (In some cases bifurcation of the rupture creates a second 'antithetic' rupture and the formation of graben on the ground surface.) The distance s of the left edge of the pile cap from the line where the rupture outcrops is a key parameter in this study. Because the exact location of the fault is not known with accuracy, even in the most recognisable eponymous faults (see Ambraseys & Jackson, 1984), s should be treated as a variable, especially in practical applications.

Finite-element modelling

The 3D model implemented in the finite-element software Abaqus (2009) is sketched in Fig. 3. The sand is represented with eight-noded hexahedral continuum elements of dimensions $d_{FE} \leqslant 1$ m. To ameliorate, if not overcome, the potential limitations of the finite-element method in reproducing shear band formation and propagation in granular materials, the largest element dimension in the vicinity of the piles is restricted to $d_{FE} = 0{\cdot}3$ m (Fig. 3(a)) – a compromise between what is believed to be the theoretical thickness of a shear band (e.g. Ambraseys & Jackson, 1984; Mühlhaus & Vardoulakis, 1987; Muir Wood, 2002) and the actual computational capabilities.

The capability of such modelling to capture realistically

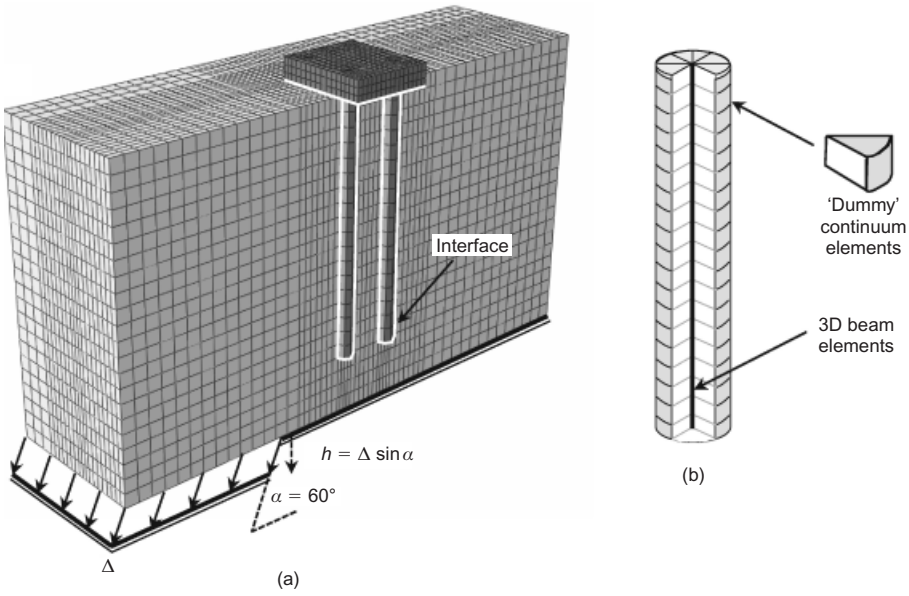

Fig. 3. (a) Finite-element half-model of the soil–foundation system; (b) 'hybrid' pile modelling

the propagation of a rupture in a deposit of sand, as well as in sand carrying surface or embedded foundations, has been demonstrated by Anastasopoulos *et al.* (2008, 2009) and Loli *et al.* (2012). Particular reference is made to the latter publication in this journal, in which the employed numerical methodology has been extensively and successfully validated through class 'A' predictions of centrifuge model tests performed at the University of Dundee, with an embedded square-in-plan caisson foundation. See also the related experimental work of Bransby *et al.* (2008a, 2008b) and Ahmed & Bransby (2009).

In the current paper, the piles are modelled with beam elements, circumscribed by eight-noded hexahedral continuum elements of nearly zero stiffness (Fig. 3(b)). The nodes of the beam elements representing the pile are rigidly connected with the circumferential solid element nodes at the same height. Thus, each pile cross-section behaves as a rigid disc. Such a hybrid modelling technique allows direct computation of pile internal forces (through the beam elements), and realistic simulation of the 3D geometry of the soil–pile interface. Both elastic and inelastic pile structural responses are simulated. In the elastic case, a Young's modulus $E = 25$ GPa is assumed, being representative of slightly cracked reinforced concrete. The piles are rigidly connected to the rigid pile cap. Sliding and detachment of the piles from the surrounding soil, an absolutely crucial requirement for this particular problem, is captured through suitable interface elements, providing a tensionless and Coulomb-type interface (of constant coefficient of friction $\tan\delta = 0{\cdot}7$). With respect to the coefficient of friction, the adopted value is considered as a reasonable assumption, capable of reproducing pile response. Because only bored piles are considered, installation effects are not expected to be of crucial importance. Although the initial stresses are likely to be different from the ones computed from gravity loading alone (e.g. Loukidis & Salgado, 2008), such effects can be approximately neglected for the problem investigated here, which is governed by the very large soil deformations.

Taking advantage of the symmetry, only half of the model is considered. The bottom boundary represents the interface between the soil and the underlying bedrock. Hence, it is split in two parts, one on the right representing the footwall that remains stationary, and the other on the left being subjected to the tectonic movement of the hanging wall. The paper considers a normal fault of a dip angle $\alpha = 60°$ and a vertical fault offset parametrically varying up to $h = 1$ m.

Before analysing the foundation–soil system, rupture propagation through the soil is analysed in the free field, that is ignoring the presence of the pile group. Then, knowing the location of the free-field fault outcrop, the group is positioned so that the (unperturbed) rupture would have emerged at distance s from its left edge (Fig. 2). In the following text, s is normalised by the width B of the group and is parametrically varied from $s/B = 0$ to 2·7. It is worth noting that because of the non-vertical rupture path even an $s/B > 1$ does not ensure that the fault will not cross the piles.

The analysis is conducted in three consecutive steps

(*a*) application of soil self-weight to simulate the initial geostatic conditions
(*b*) application of the dead load of the bridge superstructure
(*c*) application of the differential fault displacement as schematically shown in Fig. 3.

The latter is imposed in adequately small quasi-static analysis increments. The results to be presented here refer only to the additional consequences of this latter step, that is beyond the effects of gravity, and of course independently of the unavoidable dynamic effects from seismic shaking.

Soil constitutive relations

A detailed description of the Mohr–Coulomb constitutive model with isotropic strain softening used in the analyses for the dry sand can be found in Anastasopoulos *et al.* (2007). See additionally, a discussion in the 49th Rankine lecture by O'Rourke (2010), as well as a recent publication in this journal by Loli *et al.* (2012). Thus, only a brief overview is given here.

In addition to the aforementioned small element size, crucial for capturing the localisation of deformation within a relatively narrow rupture zone (the shear band) is to incorporate strain softening in the soil modelling. This is done by suitably (progressively) diminishing both the peak friction ϕ_p and dilation ψ_p angles to their residual values ϕ_{res} and 0, respectively. The model parameters are calibrated on the basis of direct shear testing. Despite its well-known short-

comings (e.g. Morgenstern & Tchalenko, 1967), which are mainly related to the non-uniformity of stresses within the soil sample, the latter remains quite popular in practice. A more detailed discussion of such issues can be found in Anastasopoulos *et al.* (2007), along with a simplified approximate procedure to estimate model parameters based on direct shear test results. That procedure has been validated in Anastasopoulos *et al.* (2007) against direct shear test results, by Gaudin (2002) in centrifuge model tests of normal and reverse fault rupturing through sand, and with trap door test results by White *et al.* (1994).

A dense sand with $\phi_p = 45^\circ$, $\phi_{res} = 30^\circ$, $\psi_p = 18^\circ$ and a loose sand with $\phi_p = 32^\circ$, $\phi_{res} = 30^\circ$, $\psi_p = 5^\circ$ are chosen for the analyses presented herein. Anastasopoulos *et al.* (2009) and much earlier Scott & Schoustra (1974) have, among others, shown that elastic–perfectly plastic constitutive soil models lead to unrealistic results, which may not even qualitatively capture the stressing of a mat foundation due to faulting; ideally plastic post-yielding behaviour not only leads to gross underestimation of bending moments, but also often fails to predict the correct mode of deformation (e.g. hogging instead of sagging). By contrast, with the adopted strain-softening model it has been repeatedly shown that the results are in reasonably satisfactory agreement with both centrifuge and reduced-scale testing for soil deposits in the free field, for rigid raft foundations and for caisson foundations (Anastasopoulos *et al.*, 2007, 2009; Loli *et al.*, 2012).

The numerical model employed here has been validated against

(*a*) centrifuge model tests of flexible steel piles in sand
(*b*) 1***g*** small-scale pushover tests
(*c*) a case history of a pile embedded in a creeping slope with a pre-existing potential sliding interface (Frank & Pouget, 2008)
(*d*) established theoretical solutions (Kourkoulis, 2009; Kourkoulis *et al.*, 2012).

Although the focus of the latter work was on slope-stabilising piles, the prevailing mechanisms are rather similar, as all of them involve piles subjected to large lateral concentrated soil deformation.

FAULT RUPTURE–SOIL–PILE INTERACTION: ELASTIC PILES

This section investigates the interplay between a quasi-statically propagating fault rupture and the pile group, assuming fully elastic (structural) pile response. Initially, free-field analysis determines the position where the fault rupture would have outcropped in the absence of the pile group. The latter is then placed at various distances relative to that location of the free-field fault outcrop, allowing a parametric exploration of different interaction mechanisms. Here results are shown for three different positions: $s/B = 2/3$, 1 and 2. Results are first presented for a fault propagating through dense sand, and a maximum bedrock offset $h = 1$ m. In the text which follows, the left row of piles are the ones that are either within, or close to, the hanging (moving) wall; the right row of piles are either within, or close to, the (stationary) footwall.

Faulting at s/B = *2/3*

In this case, the position of the group is such that, if unperturbed, the rupture would have intersected the left row of piles and emerged just in front of the right row of piles, having undergone the well-known 'refraction' (i.e. becoming steeper) upon 'entering' the soil stratum.

Figure 4 presents the 3D deformed mesh with the plastic strain contours superimposed. The presence of the group modifies the fault rupture path, forcing it to deviate upwards along the left side of the pile group (Fig. 4(a)). Notice also this deviation in the vertical and horizontal 'tomographic' sections of the finite-element model (Figs 4(b) and 4(c)), and compare the vertical sections I and II with vertical section III in the free field. At the point where rupture and pile intersect bifurcation takes place, generating a less intense shearing along a diffused antithetic rupture. The latter barely emerges on the ground surface, despite the substantial $h = 1$ m offset.

The downward movement of the hanging wall tends to downdrag the left row of piles, while the right row remains fixed in the footwall (Fig. 5(a)). However, thanks to the deviation of the fault rupture, the distress of the piles remains small even with $h = 1$ m and may be safely sustained structurally even with a (typical) reinforcement ratio of 1% (in which case the pile bending capacity $M_{RD,\rho=1\%} \approx 2{\cdot}5$ MN m). This insensitivity of the pile group to the magnitude of the fault offset is illuminated by the relationship between h and vertical displacement Δz, horizontal displacement Δx and rotation θ of the pile cap, all three of which hardly increase beyond an offset of $h \approx 0{\cdot}15$ m (Figs 5(b) and 5(c)). The interpretation is straightforward: with bedrock offset $h \approx 0{\cdot}15$ m the fault rupture has already outcropped in front of the pile group; further increase of h merely increases the height of the fault scarp, and does not further affect the pile cap displacement or rotation; the whole group is now effectively embedded in the (stationary) footwall. Internal forces in the piles are also unaffected by increases in h, although this is not shown here.

Faulting at s/B = *1*

In this case the group is positioned further to the left (i.e. towards the hanging wall), so that, if unperturbed, the fault rupture would have propagated mostly between the two pile rows and emerged at the right pile head. Now, the interplay of the piles with the emerging rupture leads to an intense bifurcation, with one fault branch appearing along the soil–pile interface of the left pile row, while the second propagates between the two pile rows and then becomes more diffused before emerging away from the group (Fig. 6(a)). As illustrated in the vertical and horizontal sections of the finite-element model (Figs 6(b) and 6(c)), the bifurcation initiates just above the pile tip (noticeable in the horizontal cross-sections D, C and B). The right branch of the fault intersects the right row at about mid-height (see horizontal section C), then for a while it propagates along the pile–soil interface, and then it finally deviates away from the group. Outside the group region, no bifurcation is observed (see vertical section III, and horizontal sections A and B): a single diffuse rupture propagates in the (more-or-less) free field at a steeper angle than α – refraction.

A significant anticlockwise rotation of the pile group takes place, generating noteworthy pile distress, accompanied by extensive soil yielding at the periphery of both pile rows along a significant portion of their length. The left row of piles is subjected to downdrag as the hanging wall moves, whereas the right piles seem to resist the movement, being essentially fixed on the footwall. As a result, the right row of piles is pushed down and the left row is pulled out.

In contrast to the previous case where the fault rupture outcropped in front, or to the left, of the pile group, now plastic deformations develop between the two pile rows. The piles suffer rather intense stressing, developing substantial bending moments, which at a few locations are of intolerable magnitude (Fig. 7(a)). One such location is the pile head of the left row of piles: M reaches 10 MN m for an

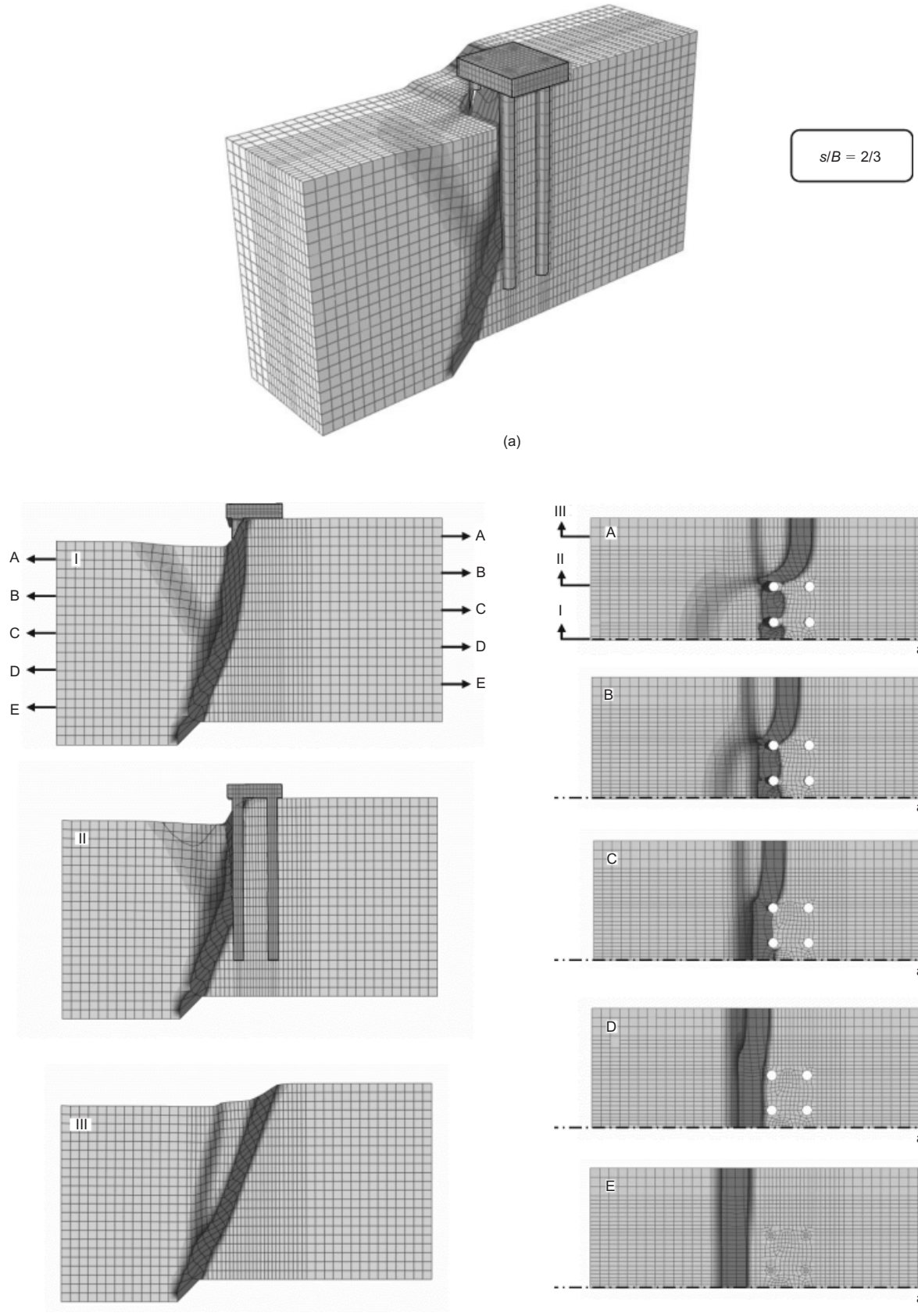

Fig. 4. Interaction of pile group with normal fault in dense sand: elastic piles, fault offset at bedrock $h = 1$ m, emergence of rupture in the free field at $s/B = 2/3$: (a) 3D deformed finite-element mesh with superimposed plastic strain contours; (b) three vertical sections: I through the centre of the group (along the x axis), II through the edge row of piles, III in the free field, 4·5d away from the group; (c) five horizontal sections, ranging from A just below the ground surface down to E just below the pile tips (a.o.s.: axis of symmetry)

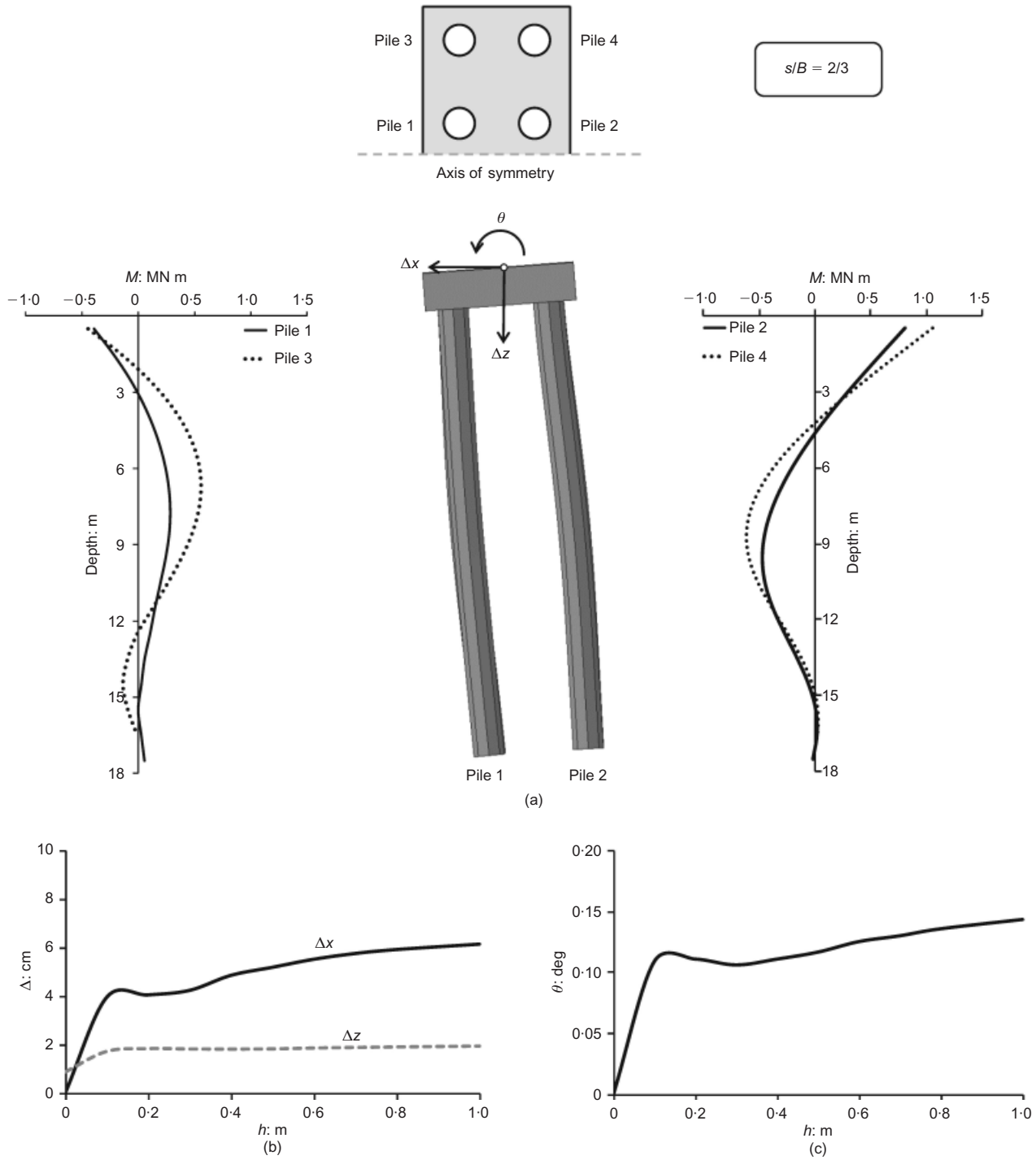

Fig. 5. Interaction of pile group with normal fault in dense sand: elastic piles, *s/B* = 2/3: (a) pile deformation, pile bending moment and deflection diagrams, for *h* = 1 m; (b) evolution with *h* of horizontal and vertical cap displacements; (c) evolution of cap rotation

offset $h = 1$ m. For relatively lightly reinforced piles (with $\rho = 1\%$), such moment demand clearly exceeds the pile capacity: $M_{RD,\rho=1\%} \approx 2{\cdot}5$ MN m. Even for the largest feasible reinforcement ratio $\rho = 4\%$ (beyond which constructability is problematic), M exceeds the pile capacity: $M_{RD,\rho=4\%} \approx 7{\cdot}5$ MN m, implying plastic hinging at the pile head of the left row. The stressing of the right pile row is milder, with the largest bending moment observed at almost mid-height. With large reinforcement ratio, say $\rho > 2{\cdot}5\%$, these piles would successfully resist the tectonic movement. With lighter reinforcement ratio (e.g. $\rho = 1\%$), however, they would not escape from failing at about mid-height.

This difference in the response of the two pile rows reveals two different developing mechanisms. In the left row, the large pile head moment stems from the downward and outward movement imposed on the piles over their entire length by the soil above the rupture plane; this pulling out of the piles creates the deformation and moment pattern seen in Fig. 7. By contrast, the right row of piles, intersected by the main rupture zone near their mid-depth, experience their largest moment just below that point of intersection. They remain essentially fixed in the (stationary) footwall below that depth, resisting with axial compression the rotation imposed by the 'downhill' movement of the normal

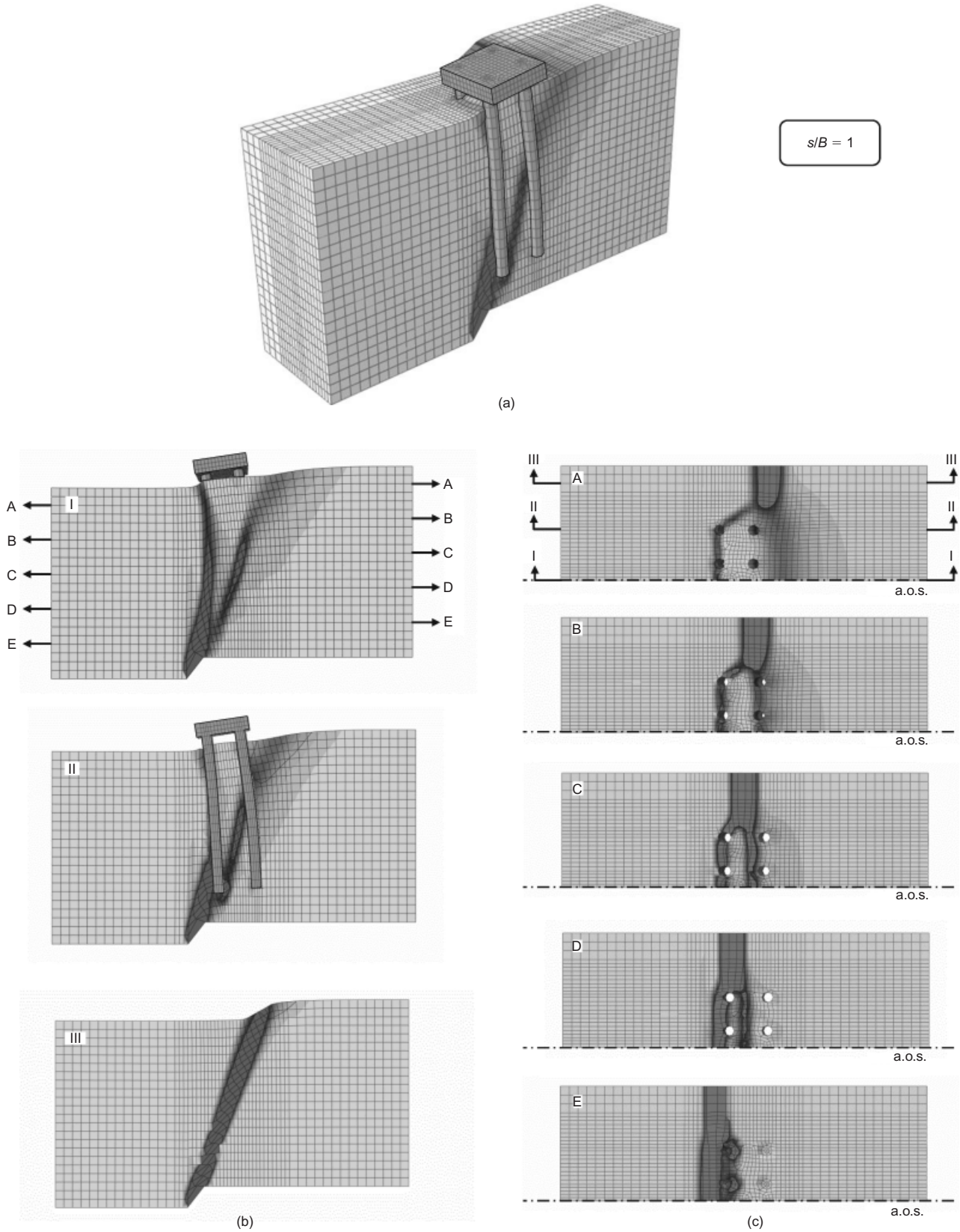

Fig. 6. Interaction of pile group with normal fault in dense sand: elastic piles, $h = 1$ m, $s/B = 1$: (a) 3D deformed finite-element mesh with superimposed plastic strain contours; (b) three vertical sections: I through the centre of the group (along the x axis), II through the edge row of piles, III in the free field, 4·5d away from the group; (c) five horizontal sections, from A just below the ground surface to E just below the pile tips (a.o.s.: axis of symmetry)

fault. To further demonstrate this behaviour, Fig. 8 depicts the distributions of axial forces, N, along the length of the left and right piles. The left piles are pulled down by the soil following the downward movement of the hanging wall, whereas the right row of piles resists, owing to its being compressed. This pulling down of the left row of piles is achieved by means of skin friction, acting on the soil–pile interface. As a result, the left piles are in tension ($N > 0$)

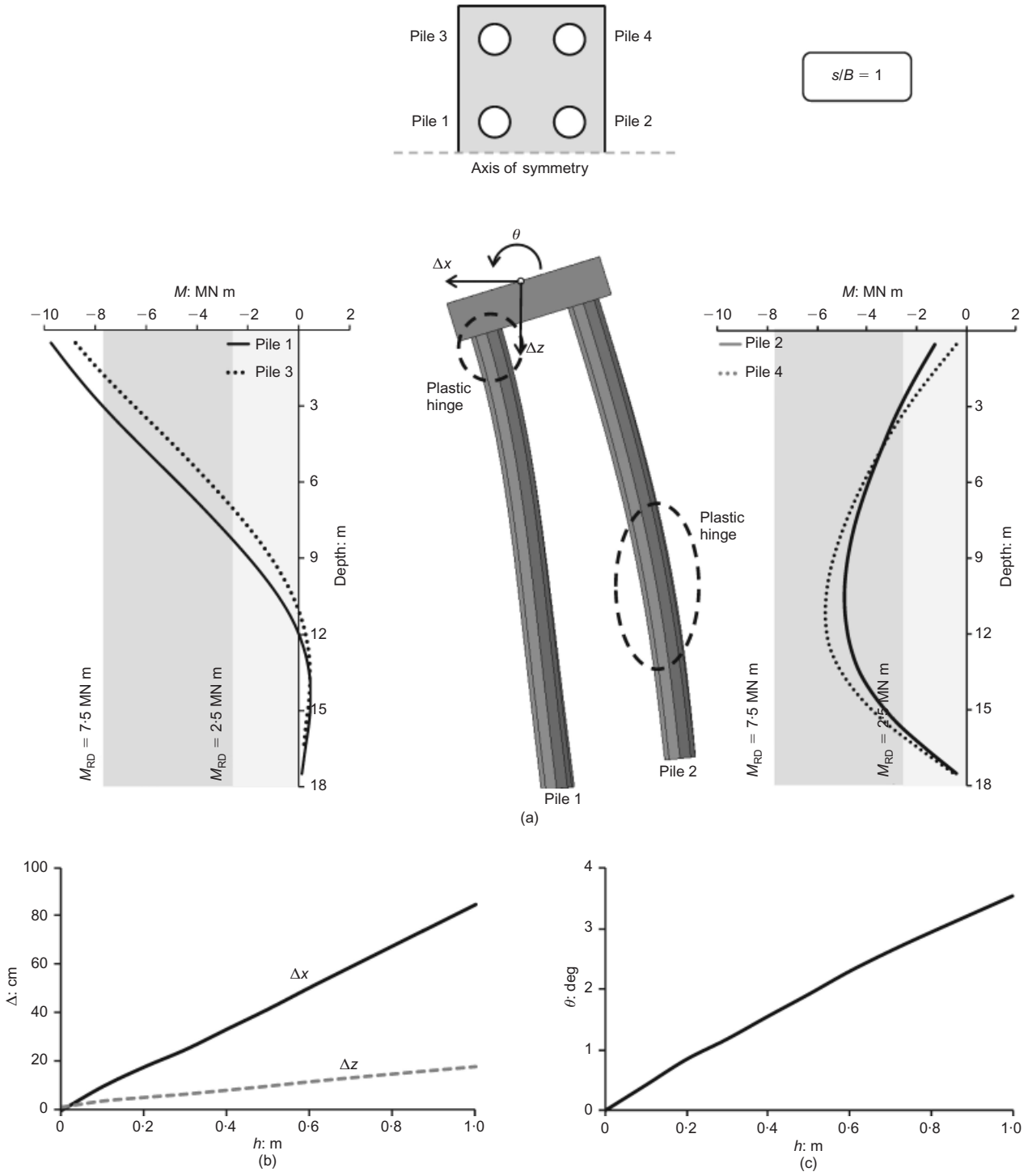

Fig. 7. Interaction of pile group with normal fault in dense sand: elastic piles, $s/B = 1$: (a) pile deformation, pile bending moment and deflection diagrams, for $h = 1$ m; (b) evolution with h of horizontal and vertical cap displacements; (c) evolution of cap rotation

over almost all of their length. A very small compressional force develops at the pile tip, which is just below the rupture path, but still within its broad shear-band zone. By contrast, the right piles are in compression ($N < 0$). Their being pulled down is firmly resisted by normal stresses at the tip. Hence, the axial compressional force is maximum at the tip and decreases on proceeding along its length owing to the downward shear tractions from the ground. (Of course, at the pile head the following equation would always apply to satisfy equilibrium.)

$$N_1 + N_3 = -(N_2 + N_4)$$

Finally notice that, contrary to the previous case, the rate of accumulation of displacement and rotation with increasing bedrock fault offset h remains nearly unchanged (Figs 7(b) and 7(c)). While for $s/B = 2/3$ the rupture deviated towards the hanging wall, leaving the group almost stationary on the footwall, now the left row (hanging wall-side) is being forced to follow the tectonic movement, pulling the pile cap along with it. This lateral-and-downward movement poses a potentially serious problem for the superstructure: differential horizontal and vertical displacements. (This sequence of events was clearly evident in the damage to the Atatturk stadium in Denizevler during the Kocaeli earthquake, as mentioned earlier.)

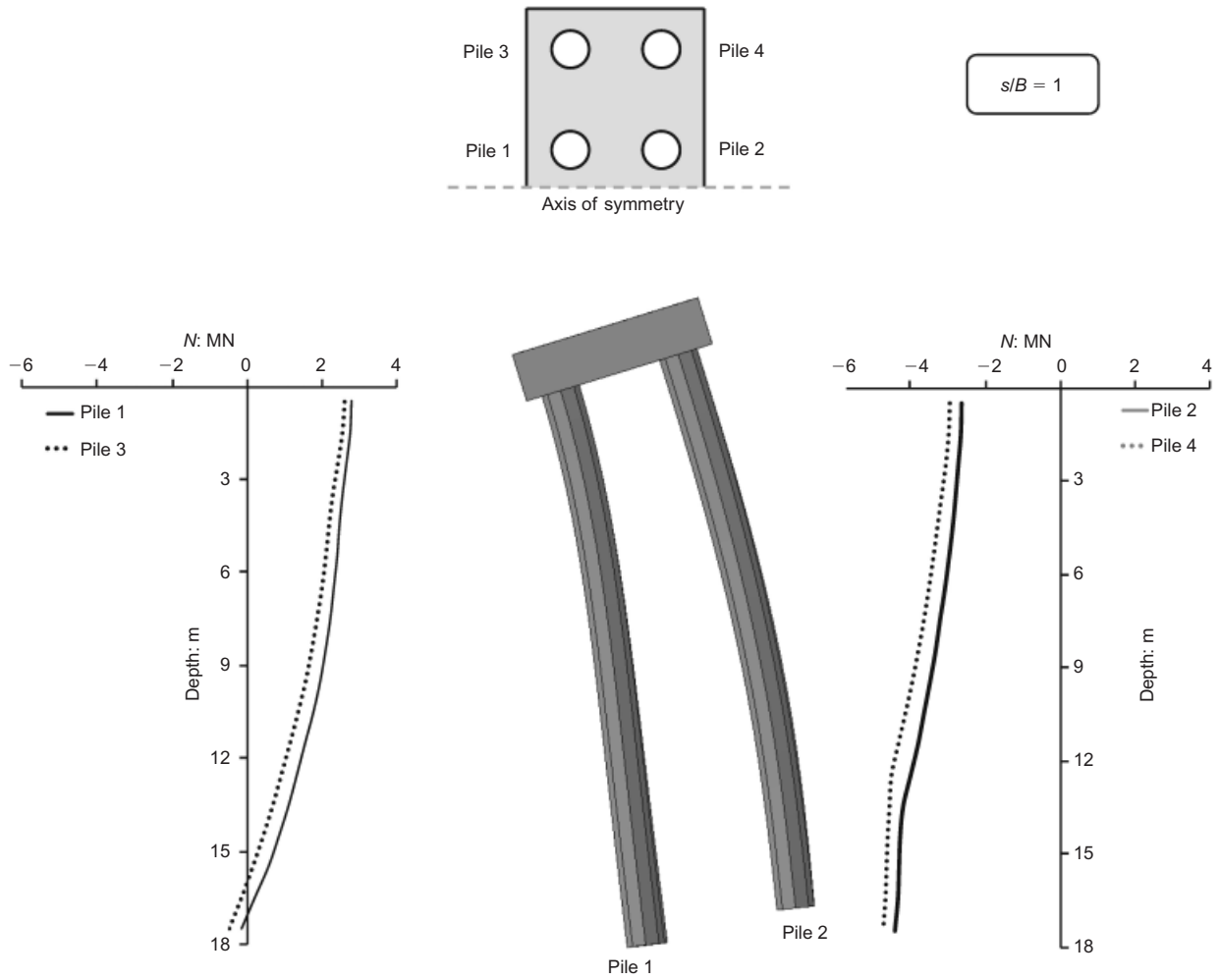

Fig. 8. Interaction of pile group with normal fault in dense sand: elastic piles, $s/B = 1$: pile deformation, a pile bending moment and deflection diagrams, for $h = 1$ m (the stressing due to dead loads has been subtracted)

Faulting at s/B = *2*

In this case the pile group is positioned even further to the left (away from the fault), so that, if unperturbed, the rupture would pass just from the tip of the right piles and outcrop well beyond the foundation. A rigid raft foundation subjected to the same fault rupture would not have felt it as a direct hit – except of course for an almost uniform downward movement as seen in Fig. 9. By contrast, with a piled foundation, an observer on the ground surface noticing the fault rupture away from the structure would have been surprised to see it sustaining substantial damage, not knowing that it was founded on piles that were in the path of the rupture. No such damage would have occurred on a surface foundation.

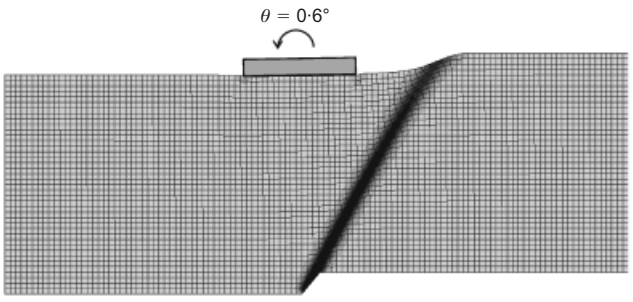

Fig. 9. Raft foundation of width $B = 10$ m subjected to $h = 1$ m faulting at $s/B = 2$

In the presence of the pile group, the main rupture zone is hardly affected, but as soon as it meets the right piles, two secondary ruptures (shear bands) are generated (Figs 10(b) and 10(c)): the first rupture (from the left) is antithetic, propagates between the two pile rows (see vertical cross-sections I and II), but is diffused before reaching the bottom of the pile cap (see horizontal sections A and B) despite the substantial offset of $h = 1$ m; the second rupture emerges at the ground surface between the right edge of the pile cap and the main outcropping rupture zone. Surprisingly, the pile cap rotates clockwise. Although the observed rotation may at first seem to be a paradox, it is rather straightforward to explain. As the main rupture plane passes just below the tip of the right row of piles, the soil exactly underneath the tip experiences intense plastic deformation (see Fig. 10(b)). As a result, the pile tip of the right row is founded on soil of reduced (remaining) resistance, experiencing loss of support. Compared to the left row of piles, which is on 'competent' soil (i.e. not affected by the fault rupture), this leads to the observed clockwise rotation. The latter may be regarded as a parasitic rotation, associated with the aforementioned loss of support, rather than with the main deformation mechanism (i.e. the downward movement of the hanging wall).

As depicted in Fig. 11(a), the flexural distress of the piles is not as intense. Yet, even in this case, the minimum considered reinforcement (of 1%) would not have been

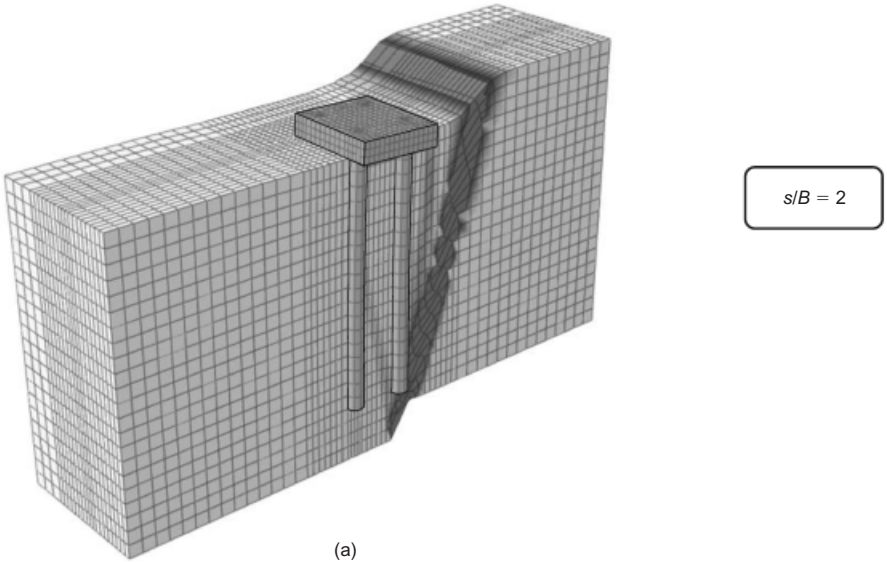

Fig. 10. Interaction of pile group with normal fault in dense sand: elastic piles, $h = 1$ m, $s/B = 2$: (a) 3D deformed finite-element mesh with superimposed plastic strain contours; (b) three vertical sections: I through the centre of the group (along the x axis), II through the edge row of piles, III in the free field, 4·5d away from the group; (c) five horizontal sections, from A just below the ground surface to E just below the pile tips

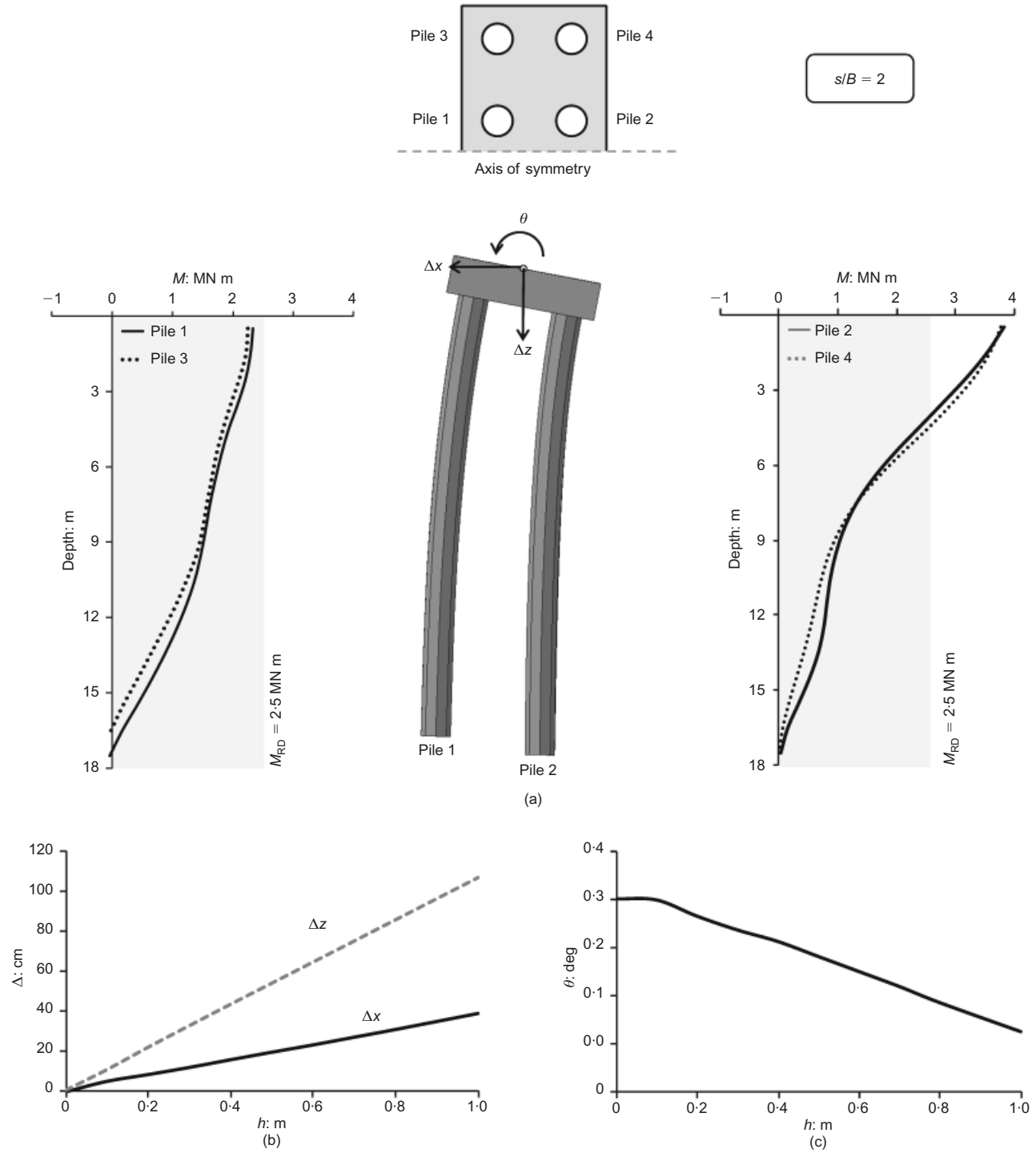

Fig. 11. Interaction of pile group with normal fault in dense sand: elastic piles, $s/B = 2$: (a) distribution with depth of pile bending moments and deflections for $h = 1$ m; (b) evolution with h of horizontal and vertical cap displacements; (c) evolution with h of cap rotation

sufficient to avoid plastic hinging of the right piles. As in the previous case, Δx, Δz and θ increase almost linearly with the imposed bedrock fault offset h (Figs 11(b) and 11(c)). It is the left piles now that offer greater resistance to downdrag, leading to the observed rotation. The distributions of axial force N along each pile, portrayed in Fig. 12 for $h = 1$ m, further elucidate the above behaviour. In complete reversal of what happens when $s/B = 1$ (previous case), it is the right piles that are in tension now (when $s/B = 2$) and the left in compression. This is directly associated with the previously discussed loss of support, as the fault rupture crosses the tip of the right row of piles.

INTERACTION MECHANISMS: INADEQUACY OF ELASTIC PILE ANALYSIS

The analyses have so far revealed that the pile group interacts intensely with the $h = 1$ m fault rupture, forcing it to divert and/or bifurcate. However, the development of such interaction mechanisms as well as the performance of the piles

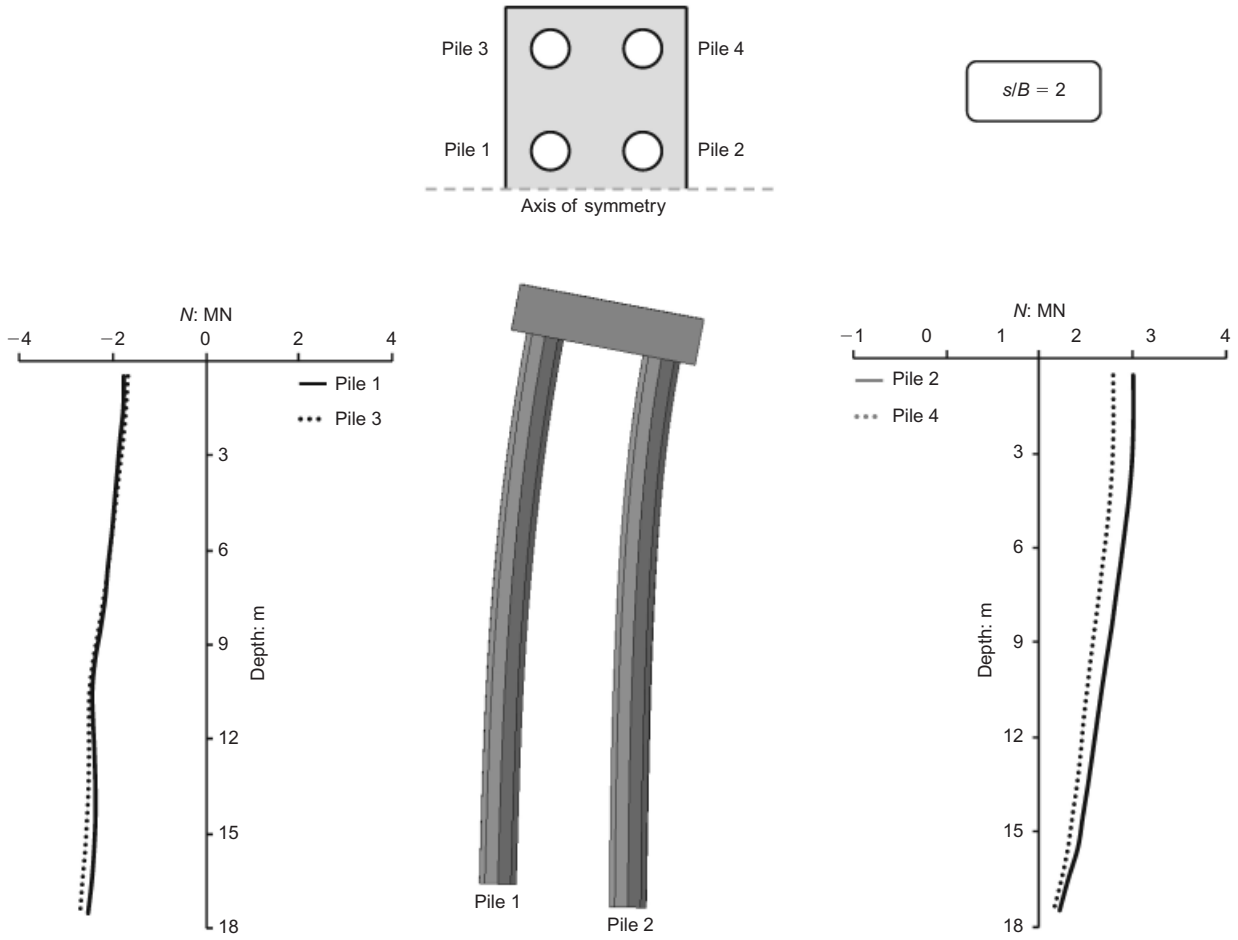

Fig. 12. Interaction of pile group with normal fault in dense sand: elastic piles, $s/B = 2$: pile deformation and distribution of pile axial forces for $h = 1$ m

(bending moments, displacement and rotation of the cap) have been shown to be functions of the position of the group relative to the fault rupture. In response to this observation, a parametric study is presented below, emphasising the mechanisms governing the response of the group.

Figure 13 summarises the role of fault rupture location, s, in pile performance for different levels of bedrock fault offset h (ranging from 0·1 to 1 m). Performance measures are the vertical and horizontal displacements of the cap, Δz and Δx, the rotation θ of the cap, as well as the maximum bending moment (for all piles, and all depths). The portrayed results are from a series of analyses with s/B varying parametrically. Three prevailing interaction mechanisms are broadly identified in Fig. 13

(*a*) mechanism A, for $0{\cdot}4 \leqslant s/B < 1$
(*b*) mechanism B, for $1 \leqslant s/B < 1{\cdot}8$
(*c*) mechanism C, for $1{\cdot}8 < s/B \leqslant 2{\cdot}7$.

Mechanism A is prevalent when the propagating fault rupture 'grazes' the left row of piles, having crossed them well above their tip (see finite-element picture labelled (1)). The main rupture path is refracted to the left, propagating along part of the boundary of the pile group. As a result, the piles remain in the footwall sustaining (relatively) limited distortion and, hence, limited pile flexural stressing. As the intersection of the fault plane becomes closer to the left pile tip, however (i.e. as $s/B \rightarrow 1$), the upper part of the group is increasingly subjected to downward and outward dragging by the moving hanging wall. Because the tips of the piles are still almost fixed on the footwall, Δz increases only moderately with increasing s/B and h. In stark contrast, both Δx (Fig. 13(b)) and θ (Fig. 13(c)) increase quite abruptly with s/B. With the upper part of the periphery of the left piles having lost much of their support on the left side, the group now acts as a retaining system of the soil mass on the right, hence an increasingly large Δx and θ, but an unaffected Δz (see also finite-element picture labelled (2)). The flexural stressing of the piles follows the same pattern as θ, increasing also quite abruptly (Fig. 13(d)).

Mechanism B prevails when the fault rupture propagates mostly between the two rows of piles, imposing rather large differential displacements – undoubtedly the worst-case scenario. As discussed, this mechanism is associated with bifurcation of the rupture zone, substantial plastic shearing (slippage) at the pile–soil interface and diffusion of plastic deformation in the immediate vicinity of the pile tips (see finite-element picture labelled (3)). With the left row being dragged downward and outward by the moving hanging wall, while the right row of piles still resists the deformation, the pile group is subjected to substantial distortion and stressing. This results in increased vertical displacement (Fig. 13(a)), as well as the largest possible horizontal displacement (Fig. 13(b)), rotation (Fig. 13(c)) and (thereby) bending moment M (Fig. 13(d)). The peak of pile distress is observed for $s/B \approx 1{\cdot}2$, in which case pile plastic hinging is unavoidable even for the maximum reinforcement ratio of 4%, even for a mere bedrock offset $h \approx 0{\cdot}2$ m.

Mechanism C governs when the fault rupture either just intersects the right piles at their tips, or barely misses them. While the whole group follows the downward and outward

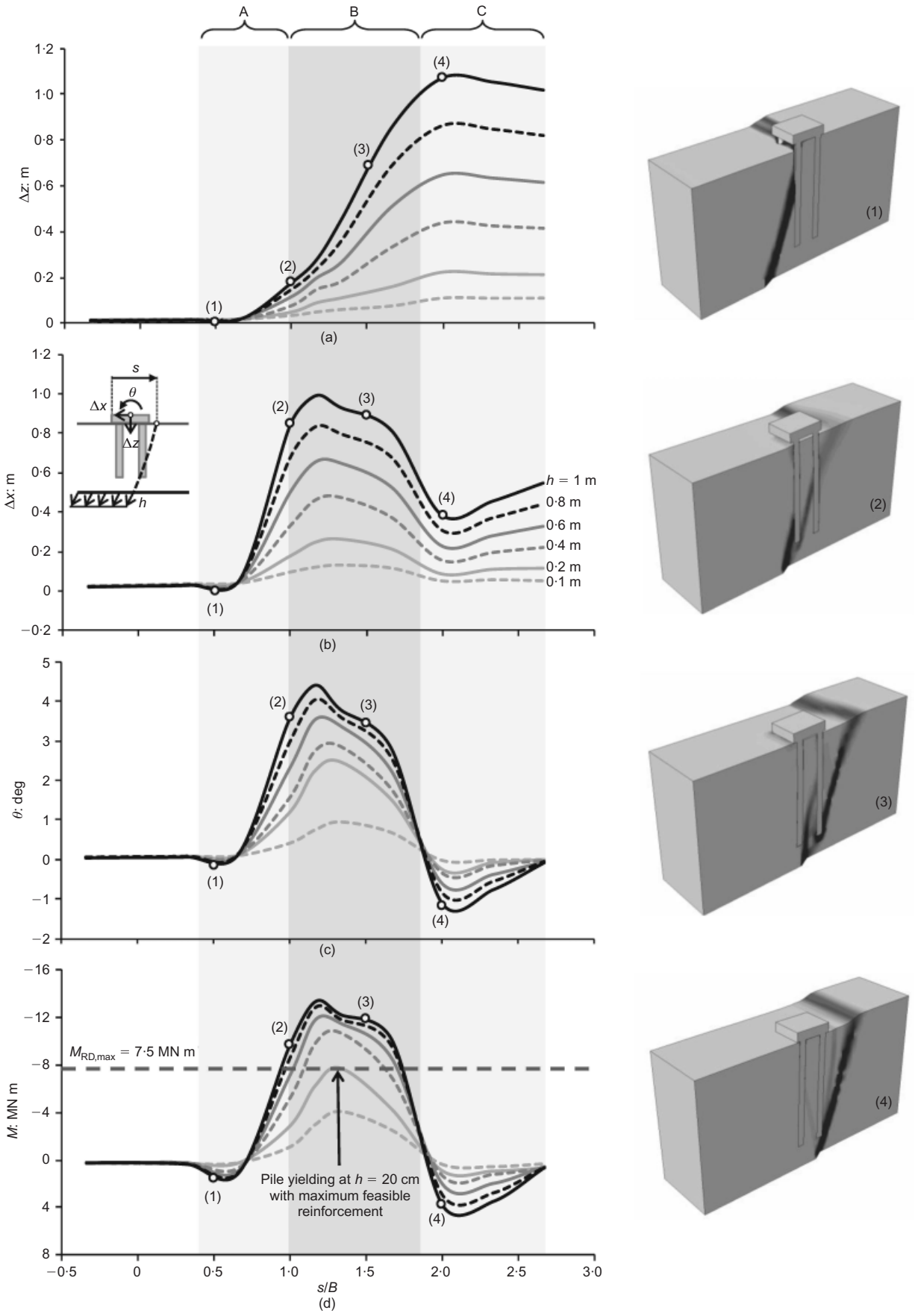

Fig. 13. Interaction of pile group with normal fault in dense sand, for elastic piles. The effect of location *s* of the fault rupture on: (a) vertical displacement; (b) horizontal displacement; (c) cap rotation; (d) maximum or minimum pile bending moments for different levels of fault offset. The shaded areas (A, B and C) refer to the three different interaction mechanisms

(to the left) translation of the hanging wall, the pile cap rotates paradoxically in the opposite direction (i.e. clockwise), as the right piles bear on the highly distressed (and hence softened) band of the rupturing fault, and essentially lose their tip bearing capacity. At $s/B \approx 2{\cdot}2$ this clockwise rotation and the associated bending moment reach their peaks. Thereafter, as the fault rupture zone moves progressively below the pile tips, the cap rotation decreases.

Eventually, beyond $s/B \approx 2{\cdot}7$ the rupture does not intersect the piles; hence it is not affected by their presence. Thus, the group moves as a (nearly) rigid body with the hanging wall. As a result

$$\Delta z \rightarrow h \qquad \text{(the vertical component of offset)} \tag{1}$$

$$\Delta x \rightarrow h/\tan 60^{\circ} \approx 0{\cdot}58h \qquad \text{(the horizontal component of offset)} \tag{2}$$

$$\theta, M \rightarrow 0 \tag{3}$$

This is almost exactly the asymptotic behaviour seen in Fig. 13.

From the above discussion it is concluded that even with the rather extreme reinforcement ratio of 4%, pile structural yielding will take place in the region of mechanism B, whenever $h > 40$ cm. In fact, for $s/B \approx 1{\cdot}3$ yielding will occur even at a mere $h = 20$ cm (Fig. 13(d)). The exact location of a fault rupture cannot be known a priori, so demanding that piles remain elastic (as seismic codes usually do for the vibratory effect of the earthquake) could only be satisfied if fault offset was less than 20 cm, unless the pile diameter was substantially larger – an expensive alternative, indeed. Hence there is a need to consider the inelastic structural behaviour of the piles. This is done in the next section.

NON-LINEAR STRUCTURAL PILE BEHAVIOUR

The non-linearity of pile response is described with moment–curvature relationships such as those of Fig. 14 for the $d = 1{\cdot}2$ m pile, heavily or lightly reinforced. Such relationships are obtained using standard cross-sectional analysis for reinforced concrete, for example by using a structural analysis code such as Xtract (Imbsen & Associates, 2004). As expected, the increase of the reinforcement ratio from 1% to 4% leads to nearly tripling of the bending moment capacity, at the expense of the pile ductility capacity (which reduces by a factor of about 2).

An illuminating comparison between elastic and inelastic structural pile response is offered in Fig. 15, referring to the

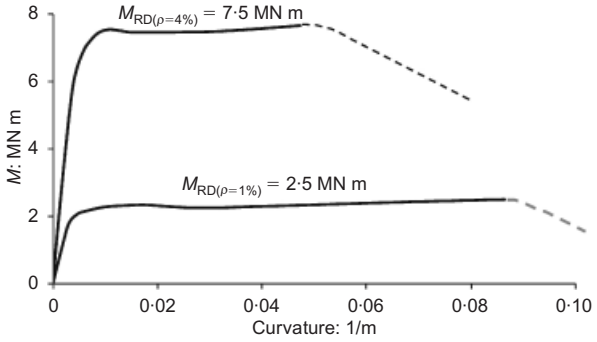

Fig. 14. Moment–curvature response of the $d = 1{\cdot}2$ m reinforced concrete piles with a small (1%) and a very large (4%) reinforcement ratio

interaction of the group with a normal fault rupture propagating through dense sand, located at $s/B = 4/3$. As already explained, when the piles behave elastically, the left row of piles (pile 1) is pulled out, forcing the right row (pile 2) to move downward, hence mobilising a bearing capacity failure mechanism at its tip. Realisation of this mechanism presumes a significant available flexural strength of the piles to be able to sustain the imposed deformation. In stark contrast, when the non-linear response of the piles is taken into account (considering a reinforcement ratio $\rho = 1\%$), plastic hinges are unavoidably formed at the pile heads. This reduces the pull-out resistance of the piles but increases the rotation of the left piles. The compression on the right piles is reduced, and there is no bearing capacity mobilisation under (and around) their tip. The penalty is a substantially larger pile cap rotation.

Figure 16 summarises the performance of the inelastic piles in dense sand subjected to normal faulting, in terms of fault outcropping location s/B and bedrock fault offset h, again for the two extreme reinforcement ratios. While the displacements Δx and Δz appear to be insensitive to pile reinforcement (and hence to pile moment capacity), the ductility demand-over-capacity ratio μ_{dem}/μ_{cap} and the rotation of the cap are fairly sensitive. Thus, the heavily reinforced pile group experiences the smallest values of ductility ratio and rotation. Whereas the lightly reinforced group may sustain $h \approx 45$ cm before the ductility capacity of the piles is exhausted, the heavily reinforced alternative can endure $h \approx 70$ cm. Notice also that the width of the zone where the piles will fail structurally drops from $0{\cdot}5B$ to $0{\cdot}3B$ from the lightly to the heavily reinforced piles.

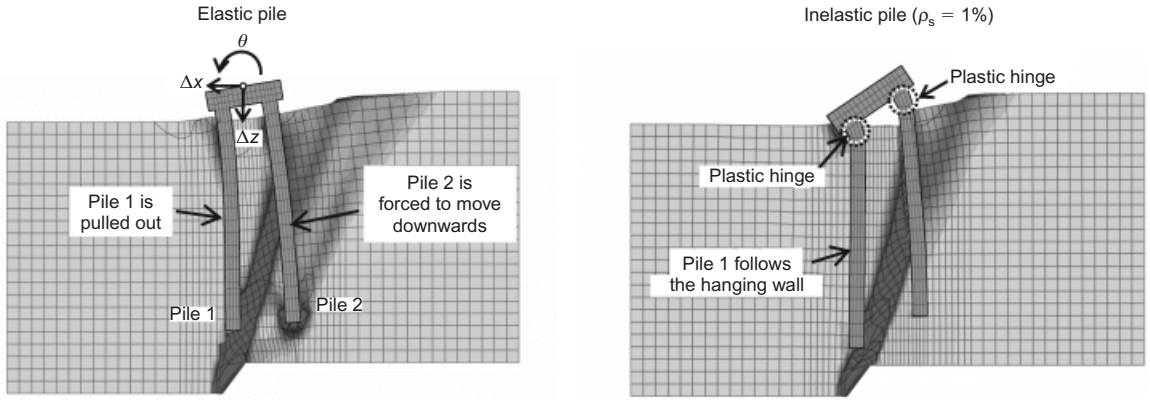

Fig. 15. Interaction of pile group with normal fault: $s/B = 4/3$, $h = 1$ m, dense sand, inelastic pile response with two different reinforcement ratios (1% and 4%): vertical section of deformed mesh with superimposed plastic strains for elastic and inelastic piles

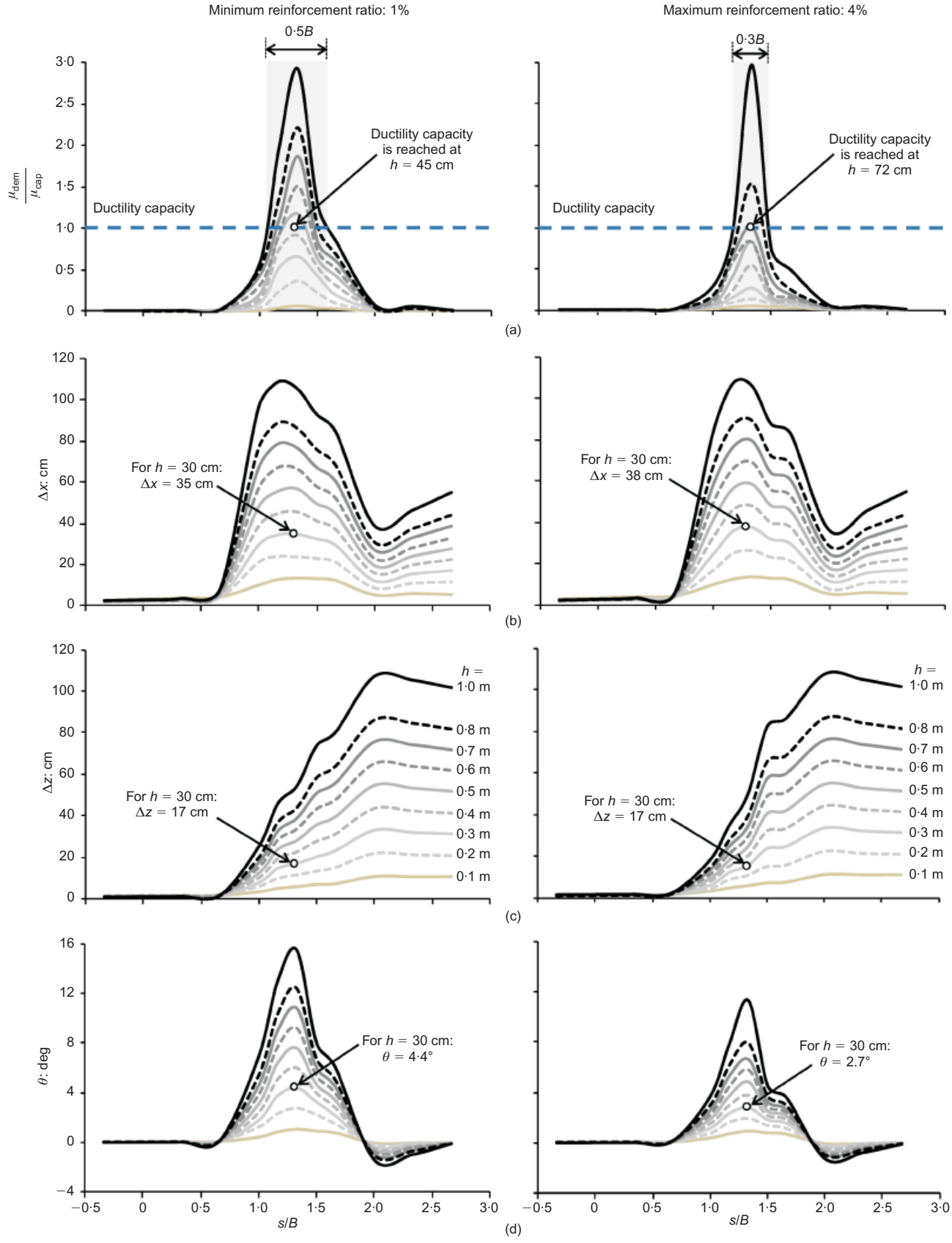

Fig. 16. Inelastic pile performance for normal faulting in dense sand, as a function of *s/B* and *h*, for two reinforcement ratios: (a) ductility demand over ductility capacity ratio; (b) horizontal cap displacement; (c) vertical cap displacement; (d) cap rotation

THE EFFECT OF SOIL DENSITY

Figure 17 summarises the performance of the pile group subjected to normal faulting through loose sand, for the two reinforcement ratios (1% and 4%), as a function of *s/B* and *h*. Again, the lightly reinforced system suffers the most, but thanks to the decreased soil stiffness and strength, even for $h = 1$ m the ductility of the piles is far from being exhausted. Compared to the response in dense sand, both

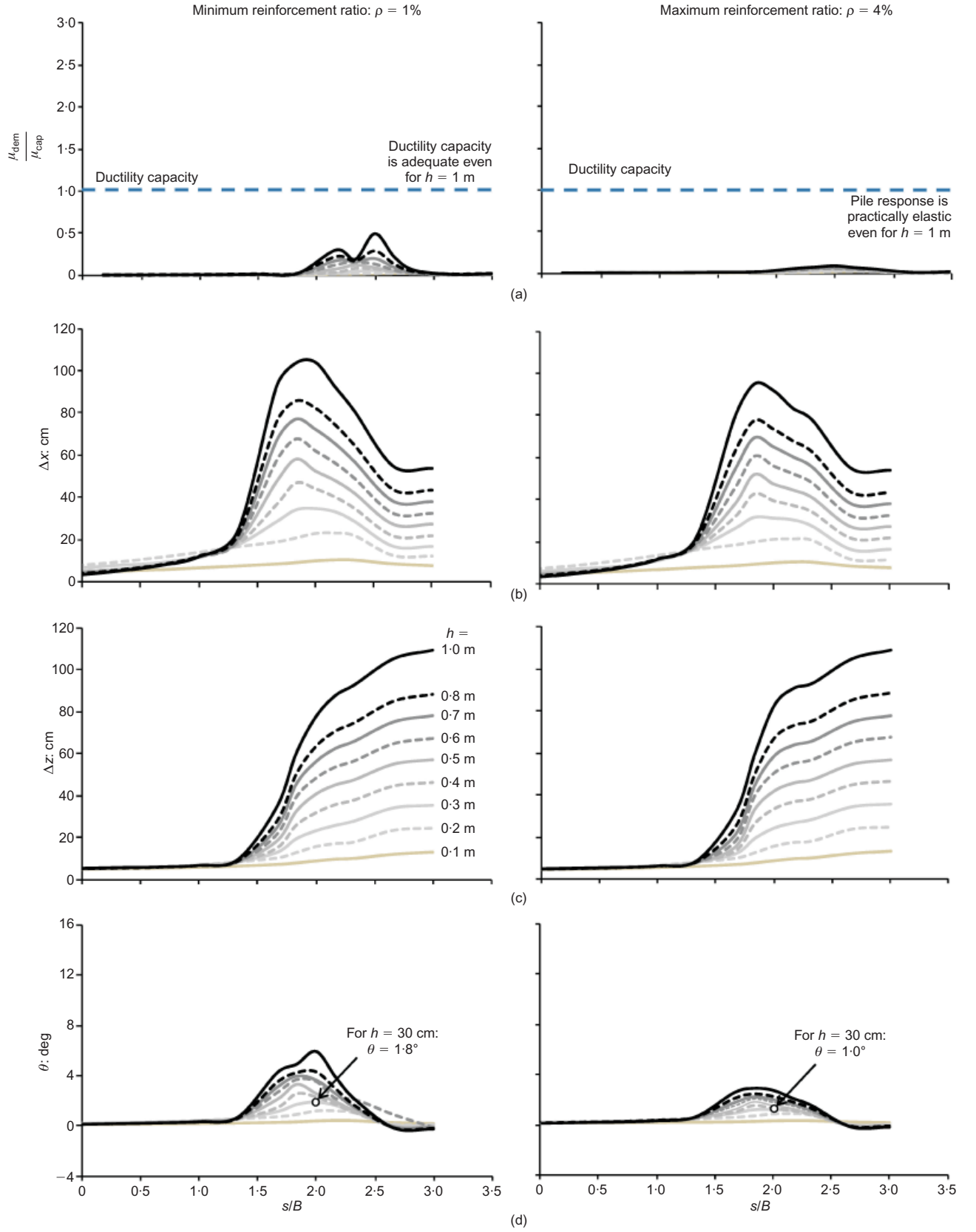

Fig. 17. Pile group in loose sand ($D_r = 40\%$). Performance as a function of *s/B* for $\rho = 1\%$ and 4%: (a) ductility demand over ductility capacity ratio for all piles; (b) horizontal cap displacement, (c) vertical cap displacement; (d) cap rotation

groups sustain substantially smaller rotation, but the differences in displacements are understandably minimal. Clearly, low soil density is beneficial for the structure.

To obtain an insight into the role of soil density, Fig. 18 compares two snapshots: one for dense sand with $s/B = 4/3$, and one for loose sand with $s/B = 2$. Because the fault rupture path is different in loose sand, the maximum distress of the pile group is observed for a different location: $s/B = 4/3$ for the dense sand (Fig. 16) but $s/B = 2$ for loose sand (Fig. 17). Hence, to focus on the worst-case scenario, the comparison is

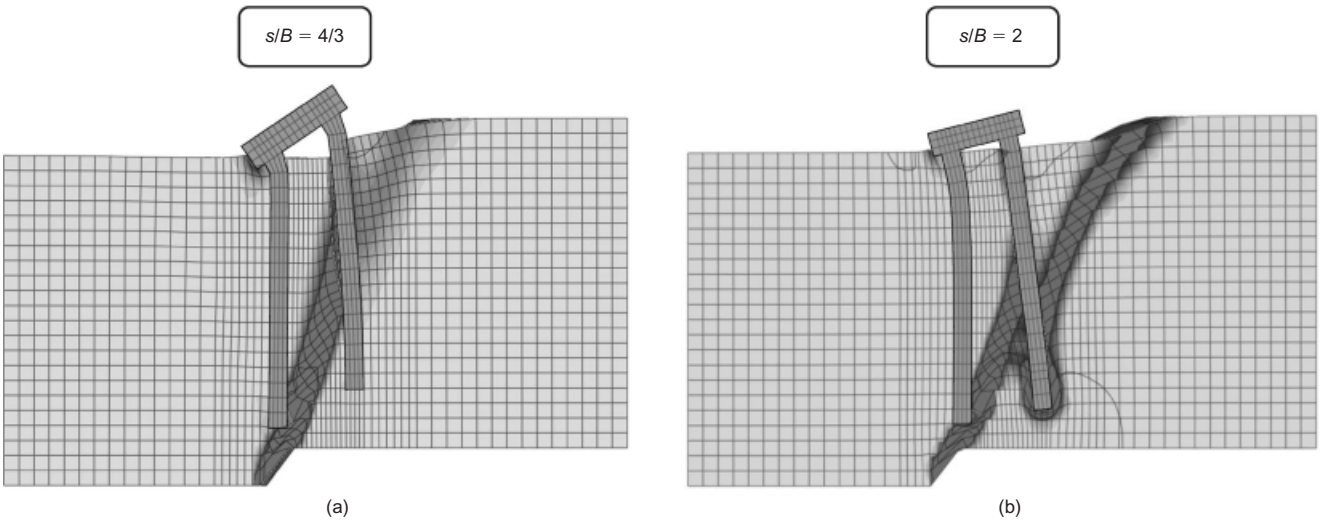

Fig. 18. Comparison of two snapshots of finite-element deformed mesh with superimposed plastic strain contours for inelastic piles: (a) dense sand, $s/B = 4/3$; (b) loose sand, $s/B = 2$ ($h = 1$ m)

made for different *s/B*. It is obvious that one of the main secrets of the success of piles in loose sand stems from the bearing capacity failure below their tip and around the lower part of the shaft of the right piles. In dense sand such failure does not take place, hence the right piles do not settle enough to reduce the rotation of the cap which is being pulled down by the left piles. In addition, the forces pulling the left piles are much reduced in the loose soil (the maximum lateral resistance per unit length of pile being proportional to the coefficient of passive resistance, $K_p = \tan^2(45^o - \phi/2)$). Hence smaller moment develops at the head of the left piles.

SUMMARY AND CONCLUSIONS

This paper has presented a numerical study of the response of a 2×4 rigidly capped pile group to deformation of the supporting–surrounding soil in the form of a propagating zone of intense shearing stemming from the tectonic offset defined at the base rock that underlies the soil stratum. The finite-element modelling and the soil constitutive relationship used in the analyses have been validated in earlier publications by extensive comparisons against centrifuge and small-scale model tests. Properly representing the ('imperfect') behaviour of the soil–pile interface was a prerequisite to a realistic simulation of pile response.

Although the paper has unavoidably focused on a specific 2×4 pile configuration, with fixed (if typical) dimensions, and a single idealised soil profile, it is believed that the observed mechanisms and the resulting pile deformation and distress are of more general (at least qualitative) validity. It is noted, however, that the present results refer to floating piles. The performance of end bearing piles would be much worse (Anastasopoulos *et al.*, 2008).

A key pervasive finding of the paper is that the performance of a piled foundation is determined by the location, *s*, of the rupturing fault and the magnitude, *h*, of the tectonic offset. Inelastic structural pile behaviour should not be disallowed, as only with extremely conservative selection of pile diameter might the response remain elastic when *h* is large.

The worst scenario for the pile group is when the propagating rupture strikes between the two rows of piles (e.g. for the range $s/B \approx 1{\cdot}0$–$1{\cdot}8$ for this specific case). Large pile cap rotation and horizontal displacement, as well as huge pile bending moments, are bound to develop. The mechanism is straightforward: the left row of piles is being pulled by the moving block of the fault (the hanging wall) while the right row of piles bears in the stationary block (the footwall). Hence, the left piles experience large bending moments at their heads, and pull the pile cap to a large horizontal displacement and an anti-clockwise rotation. The right piles resist through axial compression, and hence the cap experiences only a minor vertical displacement Δz (of the order of $h/5$). The structural design of the cap will undoubtedly be very demanding in terms of thickness and reinforcement, while the superstructure must be protected against the ensuing differential displacements. Certainly, piled foundations are hardly a solution of choice when the possibility exists of a fault to rupture between the extreme pile rows.

On the other hand, when the propagating rupture is intercepted by the front (left) row of piles it is being 'forced' to deviate upwards along these piles, to emerge in front of the group, and hence to leave all the group in the stationary block of the fault (the 'footwall'). This is a very favourable behaviour, achieved thanks to the (rigidly capped) piles. Indeed, the resulting Δx and Δz even for $h = 1$ m reach merely 6 cm and 2 cm, respectively – truly insignificant displacements given the size of the tectonic dislocation. Flexural distress of the piles is also small. Therefore, in such cases, piles (as well as deeply embedded caisson-type foundations) may offer an attractive solution.

Finally, when the fault is likely to emerge just outside the pile cap, for example about one width *B* away from the cap edge, a deep foundation such as a group of piles is hardly the best solution, because the propagating rupture may cross at least the tip of a row of piles. Thus, whereas a rigid surface raft will solely undergo a nearly uniform settlement $\Delta z \approx h$, hardly suffering any other distress, the piled foundation will suffer a measurable clockwise rotation and substantial pile bending.

The results presented in this paper will hopefully help the designer in defending the foundation–structure system against such a potential threat: the tectonic dislocation.

ACKNOWLEDGEMENTS

The work for this paper has been performed for the research project 'Dare', funded through the European Research Council (ERC) 'Ideas' Programme in Support of Frontier Research – Advanced Grant (under contract/number ERC–2–9–AdG228254–DARE).

NOTATION

B	total width of the pile cap
D	pile length
d	pile diameter
D_r	relative density
d_{FE}	minimum finite-element size
E	Young's modulus
H	depth of soil stratum
h	vertical amplitude of fault displacement at bedrock level
K_p	coefficient of pressure resistance
L	total length of pile cap
M	bending moment in a pile
$M_{RD,\rho=1\%}$	pile bending moment capacity considering 1% reinforcement ratio
$M_{RD,\rho=4\%}$	pile bending moment capacity considering 4% reinforcement ratio
N	axial force on/in a pile
s	relative position between fault rupture and foundation; defined as the horizontal distance from the left edge of the pile cap to the point of the hypothetical outcropping of the fault in the absence of foundation
α	fault angle to horizontal
Δ	offset (tectonic dislocation) at base rock
$\tan\delta$	coefficient of friction of interface
Δx	horizontal displacement of the pile cap
Δz	vertical displacement of the centre of the pile cap
θ	rotation of the pile cap
μ_{dem}/μ_{cap}	ductility demand-over-capacity ratio
ρ	reinforcement ratio
ϕ_p	peak friction
ϕ_{res}	residual friction
ψ_p	peak dilation angle

REFERENCES

Abaqus (2009). *V.6.9 user's manual*. Providence, RI, USA: Abaqus Inc.

Ahmed, W. & Bransby, M. F. (2009). The interaction of shallow foundations with reverse faults. *J. Geotech. Geoenviron. Engng, ASCE* **135**, No. 7, 914–924.

Ambraseys, N. N. & Jackson, J. A. (1984). Seismic movements. In *Ground movements and their effects on structures* (eds P. B. Attewell and R. K Taylor), Ch. 12, pp. 353–380. Guildford, UK: Surrey University Press.

Anastasopoulos, I. & Gazetas, G. (2007). Foundation-structure systems over a rupturing normal fault: Part I. Observations after the Kocaeli 1999 earthquake. *Bull. Earthquake Engng* **5**, No. 3, 253–275.

Anastasopoulos, I., Gazetas, G., Bransby, M. F., Davies, M. C. R. & El Nahas, A. (2007). Fault rupture propagation through sand: finite element analysis and validation through centrifuge experiments. *J. Geotech. Geoenviron. Engng, ASCE* **133**, No. 8, 943–958.

Anastasopoulos, I., Gazetas, G., Drosos, V., Georgarakos, T. & Kourkoulis, R. (2008). Design of bridges against large tectonic deformation. *Earthquake Engng and Engng Vibration* **7**, No. 4, 345–368.

Anastasopoulos, I., Gazetas, G., Bransby, M. F., Davies, M. C. R. & El Nahas, A. (2009). Normal fault rupture interaction with strip foundations. *J. Geotech. Geoenviron. Engng, ASCE* **135**, No. 3, 359–370.

Bransby, M. F., Davies, M. C. R., El Nahas, A. & Nagaoka, S. (2008a). Centrifuge modelling of normal fault–foundation interaction. *Bull. Earthquake Engng* **6**, No. 4, 585–605.

Bransby, M. F., Davies, M. C. R., El Nahas, A. & Nagaoka, S. (2008b). Centrifuge modelling of reverse fault–foundation interaction. *Bull. Earthquake Engng* **6**, No. 4, 607–628.

Bray, J. D. (2005). Mitigation measures against surface fault rupture. *Proc. 1st Greece–Japan Workshop on Seismic Design, Observation, and Retrofit of Foundations, Laboratory of Soil Mechanics, Athens* (eds G. Gazetas, Y. Goto and T. Tazoh).

Bray, J. D., Seed, R. B., Cluff, L. S. & Seed, H. B. (1994a). Earthquake fault rupture propagation through soil. *J. Geotech. Engng, ASCE* **120**, No. 3, 543–561.

Bray, J. D., Seed, R. B., Cluff, L. S. & Seed, H. B. (1994b). Analysis of earthquake fault rupture propagation through cohesive soil. *J. Geotech. Engng, ASCE* **120**, No. 3, 562–580.

Cole, D. A. Jr. & Lade, P. V. (1984). Influence zones in alluvium over dip-slip faults. *J. Geotech. Engng, ASCE* **110**, No. 5, 599–615.

Faccioli, E., Anastasopoulos, I., Callerio, A. & Gazetas, G. (2008). Case histories of fault–foundation interaction. *Bull. Earthquake Engng* **6**, No. 4, 557–583.

Frank, R. & Pouget, P. (2008). Experimental pile subjected to long duration thrusts owing to a moving slope. *Géotechnique* **58**, No. 8, 645–658, http://dx.doi.org/10.1680/geot.2008.58.8.645.

Gaudin, C. (2002). *Experimental and theoretical study of the behavior of supporting walls: Validation of design methods*. PhD thesis, Laboratoire Central des Ponts et Chaussées, Nantes, France.

Imbsen & Associates (2004). *XTRACT – Cross section analysis program for structural engineers*, Version 3.0.3. Sacramento, CA, USA: Imbsen & Associates Inc.

Kawashima, K. (2001). Damage of bridges resulting from fault rupture in the 1999 Kocaeli and Düzce, Turkey, earthquakes and the 1999 Chi-Chi, Taiwan earthquake. *Proceedings of workshop on seismic fault-induced failures* (eds K. Konagai, M. Hori and K. Meguro), pp. 171–190. Tokyo, Japan: University of Tokyo Press.

Kourkoulis, R. (2009). *Interplay of raft foundations and piles with a failing slope*. PhD thesis, Laboratory of Soil Mechanics, National Technical University, Athens, Greece.

Kourkoulis, R., Gelagoti, F., Anastasopoulos, I. & Gazetas, G. (2012). Hybrid method for analysis and design of slope stabilizing piles. *J. Geotech. Geoenviron. Engng, ASCE* **137**, No. 1, 1–14.

Lade, P. V., Cole, D. A. & Cummings, D. (1984). Multiple failure surfaces over dip-slip faults. *J. Geotech. Engng, ASCE* **110**, No. 5, 616–627.

Loli, M., Bransby, M. F., Anastasopoulos, I. & Gazetas, G. (2012). Interaction of caisson foundations with a seismically rupturing normal fault: centrifuge testing versus numerical simulation. *Géotechnique* **62**, No. 1, 29–43, http://dx.doi.org/10.1680/geot.9.P.153.

Loukidis, D. & Salgado, R. (2008). Analysis of the shaft resistance of non-displacement piles in sand. *Géotechnique* **58**, No. 4, 283–296, http://dx.doi.org/10.1680/geot.2008.58.4.283.

Morgenstern, N. R. & Tchalenko, J. S. (1967). Microscopic structures in kaolin subjected to direct shear. *Géotechnique* **17**, No. 4, 309–328, http://dx.doi.org/10.1680/geot.1967.17.4.309.

Muir Wood, D. (2002). Some observations of volumetric instabilities in soils. *Int. J. Solids Structs* **39**, No. 13–14, 3429–3449.

Mühlhaus, H. B. & Vardoulakis, I. (1987). The thickness of shear bands in granular materials. *Géotechnique* **37**, No. 3, 271–283, http://dx.doi.org/10.1680/geot.1987.37.3.271.

O'Rourke, T. D. (2010). Geohazards and large, geographically distributed systems. *Géotechnique* **60**, No. 7, 505–543, http://dx.doi.org/10.1680/geot.2010.60.7.505.

Scott, R. F. & Schoustra, J. J. (1974). Nuclear power plant sitting on deep alluvium. *J. Geotech. Engng Div., ASCE* **100**, No.4, 449–459.

Ulusay, R., Aydan, O. & Hamada, M. (2002). The behaviour of structures built on active fault zones: Examples from the recent earthquakes of Turkey. *Structl Engng Earthquake Engng, Japan. Soc. Civ. Engrs* **19**, No. 2, 149–167.

White, R. J., Stone, K. J. L. & Jewel, R. J. (1994). Effect of particle size on localization development in model tests on sand. *Proceedings of the international centrifuge conference* (eds C. F. Leung, F. H. Lee and T. S. Tan), pp. 817–822. Rotterdam, the Netherlands: Balkema.

Youd, T. L., Bardet, J.-P. & Bray, J. D. (2000). Kocaeli, Turkey, earthquake of August 17, 1999 reconnaissance report. *Earthquake Spectra* **16**, Suppl. A, 456.